An Automatic Optic Disk Detection and Segmentation System using Multi-level Thresholding

Bahadir KARASULU
Department of Computer Engineering, Faculty of Engineering, Canakkale Onsekiz Mart University, Terzioglu Kampusu,17020, Canakkale, Turkey
bahadirkarasulu@comu.edu.tr

***Abstract*—Optic disk (OD) boundary localization is a substantial problem in ophthalmic image processing research area. In order to segment the region of OD, we developed an automatic system which involves a multi-level thresholding. The OD segmentation results of the system in terms of average precision, recall and accuracy for DRIVE database are 98.88%, 99.91%, 98.83%, for STARE database are 98.62%, 97.38%, 96.11%, and for DIARETDB1 database are 99.29%, 99.90%, 99.20%, respectively. The experimental results show that our system works properly on retinal image databases with diseased retinas, diabetic signs, and a large degree of quality variability.**

***Index Terms*—image processing, image segmentation, biomedical imaging, digital imaging, retinal image database.**

I. INTRODUCTION

In ophthalmic image processing research area, for qualifying the retina lesions, the Optic Disk (OD) detection is important because the major retinopathologies (e.g., exudates and/or drusen) and other abnormalities (based on the hypertensive retinopathy, and the cottonwool spots) frequently appear in color fundus (i.e., retina) images as clusters of regions with their size and pixel intensities comparable to the OD [1, 2]. According to Niemeijer et al. [3], OD is a significant nerve area of the retina that the retinal vasculature enters and leaves the eye-ball on this area. In this way, the OD area indicates the exit point of the ganglion cell axons to form the optic nerve of the eye. In the literature, the OD detection techniques are classified by some studies into several groups [4]. These groups are often based on template matching [5], active contour modeling (ACM) (e.g., snake method) [6], multi-level thresholding [7], machine learning [8], and etc [4].

According to the Welfer et al. [2], the common features such as region size and pixel intensities are unreliable for segmenting the OD. Welfer et al. [2] divided the methods related to the OD in the literature into two main categories: the methods for detection of OD location without OD boundary, and the methods for detection of OD locus with OD boundary. It should be noted here, the former do not segment the OD, but the latter segment the OD [2]. In the literature, a lot of studies are focused on the detection and segmentation (D&S) of OD for diagnosis of retinopathologies [9-11].

The basic objective of thresholding technique is to classify pixels into two or more classes which are determined by the background and one (or more) object(s) in given scene of image. Bi-level thresholding separate image into one foreground and one background regions that it is a simple segmentation process. By the way, its computational time is reasonable. However, when this thresholding process is extended to multi-level thresholding, the computation time grows exponentially with the number of thresholds. In segmentation of complex images, using a multi-level threshold method has become a necessity. According to Ng [12], the global thresholding determines a single threshold value from the histogram of the given image, but local thresholding employs localized gray-level information to choose multiple threshold values that each one is optimized for a small region in the given image. In addition, the former can deal with uniform illumination cases, but the latter can deal with non-uniform illumination cases.

Furthermore, image thresholding methods can be divided into two main groups: parametric and non-parametric approaches [13]. According to Huang et al. [13], a statistical model is first assumed to fit the gray level distribution of given image. Also, a set of parameters controls the fitness of model. These parameters are determined by using the histogram. In addition, in non-parametric methods, the thresholds are chosen by optimizing an objective function. In this frame, Otsu method is a simple technique and based on the discriminant analysis. According to Huang et al. [13], among the bi-level thresholding studies, Otsu's method [14] is a very popular non-parametric thresholding technique. Otsu method can be easily extended to a multi-thresholded (multi-level) version. Bi-level version of Otsu method is based on the iterations of the zeroth- and first-order cumulative moments of a gray level histogram [13]. Multi-level Otsu thresholding process is an extension to the original Otsu thresholding process. It works very well for objects with colored or complex backgrounds, for which bi-level Otsu thresholding fails to produce satisfactory results. It determines more than one threshold for a given image.

In our study, in order to segment the region of OD, we developed a segmentation approach based on multi-level thresholding. It involves a multi-level Otsu thresholding followed by connected component analysis (CCA). The main advantages of this approach is the automatic cluster determination, and it completely avoids the heavy computational costs. The D&S system based on our approach takes given RGB image as input image, and also, a Karhunen-Loève transformation (KLT) is performed on the

Digital Object Identifier 10.4316/AECE.2014.02025

R, G and B channels to determine energy values of given image. KLT represents images respecting their spatial properties. Therefore, the segmentation process is then applied on the image component (i.e., channel) that contains most of the energy. In addition, the related morphological operations are used to correctly determine OD boundary with help of the eccentricity (i.e., roundness) value of given blob areas in given mask (i.e., bi-level segmented) image. Then, our system produces the final edge-based segmentation result of OD region.

The main difficulties in OD D&S are the high similarities with other large bright lesions (e.g., cottonwool spots). There are many publicly available retinal image databases in the literature, where any proposed system should be validated. The performance results of a D&S system can be considered as a meaningful result in this research field, if its efficiency can be approved based on testing on several and inhomogeneous retinal image datasets.

In our study, the experiments were conducted on 40 images collected from DRIVE database [15], and 81 images collected from STARE database [16] and 89 images collected from DIARETDB1 database [17]. DRIVE database contains 20 test images and 20 training images of good quality without serious lesions. The STARE and DIARETDB1 databases contain retinal images with diseased retinas, diabetic signs, and have a large quality variability (e.g., illumination problems).

In this study, we focus challenging two current kinds of approaches, which are detection of OD and segmentation of OD region. Especially, our system integrates the process of OD detection with the process of OD segmentation together. The proposed D&S approach consists of a set of some methods such as median filter, KLT, multi-level Otsu's thresholding and Sobel edge detection. It is able to deal with different illumination and noise conditions, and also, it can be applied in pathological images and in most of them it worked well. Sobel method finds the edges in an image using the Sobel approximations of the derivatives for changes in horizontal and vertical directions. Therefore, it precedes the edges at the related points where the gradient has the highest value.

The main contribution of this work is to develop an automatic system for unsupervised D&S of OD from fundus (i.e., retinal) images and to evaluate its performance via several metrics commonly used in information retrieval. In the current system, a multi-level thresholding process based on the automatic clustering approach is used to accurately determine the OD localization and to correctly segment the OD boundary without requiring heavy computational costs.

The rest of the paper is organized as follows: Section II represents the related work in the literature, and also, it describes the details of three well-known retinal image databases in the literature. In Section III, our proposed approach and its implementation (i.e., the D&S system) for OD detection and OD segmentation are explained. The experimental results of our D&S system obtained with three retinal image databases are presented in Section IV. Finally, Section V concludes the paper.

II. Related Work

For detection and/or segmentation of OD, there are a lot of studies in the literature. Siddalingaswamy and Gopalakrishna [9] studied on automatic localization and accurate boundary detection of OD. In their study, an iterative thresholding method followed by CCA is applied to find an approximate center of OD. Therefore, an ACM is used to determine the exact boundary of OD. They tested their method via an image database consists of 148 retinal images and compared with human expert's decisions. The experimental results in their study show that the OD localization accuracy is 99.3%, and also, sensitivity and specificity measurements of boundary detection of OD in terms of mean and standard deviation are 90.67%±5.05 and 94.06%±6.83, respectively. In their experiments, OD boundary labelled by human expert for all images is used as ground-truth (GT) data.

Köse et al. [10] developed an alternative approach to detect diabetic retinopathy (DR). It is built on the inverse segmentation method. In their study, background image approach along with inverse segmentation is applied to measure and track the degenerations in color fundus images. According to Köse et al. [10], direct segmentation techniques produce unsatisfactory results in some conditions caused by the inhomogeneous texture of unhealthy areas (e.g., DR regions). Therefore, an inverse method is proposed to exploit the homogeneity of healthy areas rather than dealing with varying structure of unhealthy areas for bright lesions' segmentation (e.g., hard exudates and cottonwool spots). In addition, they developed a complete segmentation system for several retinopathologies such as DR and abovementioned bright lesions. The performance of the segmentation system is tested on different datasets of color fundus images selected at various qualities. Hence, the experimental results in their study show that the performance is over 95% in detection of the OD, and 90% in segmentation of the DR.

Muramatsu et al. [11] compared three different methods in their study that employed ACM, fuzzy c-means (FCM) clustering, and artificial neural network (ANN) for OD region's segmentation. The experimental results show that the overall disc segmentation results using ACM and ANN were comparable and slightly better than that of FCM.

Youssif et al. [18] presented a method to automatically detect the position of the OD in digital retinal fundus images. The proposed method starts by normalizing luminosity and contrast throughout the given image. In addition, the OD-center detection is based on the segmented retinal blood vessels. These vessels are segmented using a simple matched filter. The experimental results show that the OD-center was detected correctly in 98.77% for STARE database and in 100% for DRIVE database as well.

Niemeijer et al. [19] presented a method that determines whether a macula centered retinal image is from the left or right eye. The method automatically detects the OD, the fovea and the vascular arch. Its algorithm relies on a specific energy function. A combination of optimization methods was used to minimize the energy function. They used 220 different macula centered digital color fundus photographs in their experiments. Their proposed system localizes the OD in 91% of all cases, the fovea in 94% of all cases, and

correctly positions 74% of all vessel landmarks.

Walter and Klein [20] presented new algorithms based on mathematical morphology for the detection of OD and the vascular tree. They first found the OD position approximately, then the exact contours of ODs in given images were found by means of the watershed transformation. They tested the algorithm that is based on morphological operators. The test conducted on 30 color images, and in 27 images, their algorithm found the exact contours of ODs.

Qureshi et al. [21] proposed an efficient combination of algorithms for the automated localization of the OD and macula in retinal fundus images. They showed that their combination outperformed all the individual algorithms. The number of outputs of the algorithms falling in a specified radius circle is counted by a weighted linear combination and majority voting based scheme. This circle is marked as a hotspot. Their method achieved highest performance. The experiments are conducted on three different public databases. The combined system's OD detection performance results are 96.79% for DIARETDB0 database, 94.02% for DIARETDB1 database, and 100% for DRIVE database. The total average of performance results is 96.34% that achieved by the combined system.

Morales et al. [22] presented a method that automatically segments the OD from a fundus image. Their proposed method is based on mathematical morphology along with principal component analysis. The method makes use of different operations such as a variant of the watershed transformation (i.e., generalized distance function), the stochastic watershed, and geodesic transformations. The experiments are conducted on five public databases. The average values for performance results are obtained by Jaccard's and Dice's coefficients of 0.8200 and 0.8932, respectively, by an accuracy of 0.9947, and by a true positive and false positive fractions of 0.9275 and 0.0036.

Welfer et al. [23] presented a new adaptive morphological method for the automatic detection of the OD in digital color eye fundus images. The method has been designed to detect the OD-center and the OD-rim (i.e., boundary). The experiments were conducted on the DRIVE database and DIARETDB1 database. In these experiments, their proposed method was able to detect OD-center with 100% and 97.75% of accuracy, respectively. They considered correct all automatically detected OD location that is within the borders of the OD marked manually. The OD-rim was detected on the DRIVE database with average sensitivity and specificity of 83.54% and 99.81%, respectively, and on the DIARETDB1 database with average sensitivity and specificity of 92.51% and 99.76%, respectively.

Liao et al. [24] proposed a faster version of Otsu's method for improving the efficiency of computation for the optimal thresholds of an image. At first, for image segmentation, they proposed a criterion for maximizing a modified between-class variance that is equivalent to the criterion of maximizing the usual between-class variance. Hence, they designed a recursive algorithm to efficiently find the optimal threshold. However, this procedure produces the same set of thresholds as the original method. The experimental results of their study show that the computational time with the use of new criterion takes less computation to compute both the cumulative probability (zeroth-order moment) and the mean (first-order moment) of a class. According to the experimental results of a five-level (multi-level) threshold selection, their proposed method can reduce down the processing time from more than one hour by the conventional Otsu's method to less than 107 seconds [24].

The accurate D&S of OD is apparently useful in some cases, such as for glaucoma diagnosis, in which the diameter of OD increases. Frequently, color fundus images present great inter- and intra-image variability, and noise, poor contrast and brightness, which affect the performance of many detection and/or segmentation system.

The main motivation in our study is to develop an automatic system for D&S of OD, which has accurate D&S of OD performance results in abovementioned conditions, and works with lower computational complexity. The procedure of our D&S approach is implemented in a user-friendly system which is able to deal with different parameters that can be useful when applied on new retinal images selected from large datasets. These parameters are used to refine the search of the OD region in a given image, in which some rough or very small blob areas partly similar to the OD region reside too. As far as we know, there is no any similar system in the literature, which shows good performance in D&S of OD region in images of three public retinal image databases (i.e., DRIVE, STARE and DIARETDB1) at the same time.

A. Retinal image databases

Any OD D&S system should be tested on one or more publicly available retinal image databases for optic nerve evaluation. In other words, the robustness of the proposed system must be evaluated under various situations, such as varying illumination and acquisition conditions, and different diabetic lesions.

In our study, we used the DRIVE (Digital Retinal Images for Vessel Extraction) database [15, 25], the STARE (STructured Analysis of the Retina) database [16], and DIARETDB1 (Standard Diabetic Retinopathy DataBase Calibration level 1) database [17], which are publicly available color retinal image databases.

The first dataset used in our experiments consists of a total of 40 color fundus photographs collected from DRIVE database. According to Fraz et al. [26], these fundus photographs were obtained from a DR screening program that its population consisted of 453 subjects between 31 and 86 years of age. Considering the database images, 33 are normal and 7 contain the signs of pathology, e.g. exudates, hemorrhages and pigment epithelium changes. Each image in the database has been JPEG compressed [26], and is of size 584 x 565 pixels, represented using 24 bits per pixel in the standard RGB format. They were acquired using a Canon CR non-mydriatic camera with three charge-coupled device (CCD) detectors. The camera has a Field of View (FOV) of 45 degrees for images. The photographs are low-resolution fundus images of the retina, having an approximate spatial resolution 20 μm per pixel [25]. According to the study of Zhu et al. [25], the results of manual segmentation of the blood vessels are provided for all 40 images in the dataset; however, no information on the optic nerve head (i.e., OD) is available.

The second dataset used in our experiments is a subset of the STARE Project's database [16]. The subset contains 81 fundus images that were captured using a TopCon TRV-50 fundus camera at FOV of 35 degrees. These images were digitized at 605 x 700 pixels, and represented using 24 bits per pixel. This dataset contains 31 images of normal retinas and 50 images at diseased retinas [18]. The OD is visible in all 81 images, although in 14 images it is on the border of the image so that only a fraction of the OD is visible. In addition, in five of 81 images, OD is completely obscured by hemorrhaging. The information on the optic nerve head (i.e., OD) is available as OD-center coordinates on the given text file. Especially, these 81 images have been selected from the full set of raw images (circa 400 images) in the STARE database, in which a variety of retinal diseases, confusing lesions and manifestations (i.e., bright circular lesions similar to the OD) frequently exist.

The third dataset used in our experiments consists of a total of 89 color fundus images collected from the DIARETDB1 database. These images are of size 1500 x 1152 pixels, with 24 bits per pixel [17]. In addition, 84 of them contain at least mild non-proliferative signs (i.e., microaneurysms) of the DR. Furthermore, five of them are considered as normal which do not contain any signs of the DR [22].

III. The Proposed Approach

In our study, an automatic (i.e., unsupervised) OD D&S system is proposed. The infrastructure of this system uses some methods and techniques in order to detect and segment the OD in color retinal images such as KLT, Otsu's multi-level thresholding, morphological operations, CCA and the Sobel edge detection technique. In the following subsection, the infrastructure of our system is explained in details.

A. Automatic detection and segmentation system

In Fig. 1, the flowchart of the proposed system is shown. In the figure, related steps are given as an abstract form.

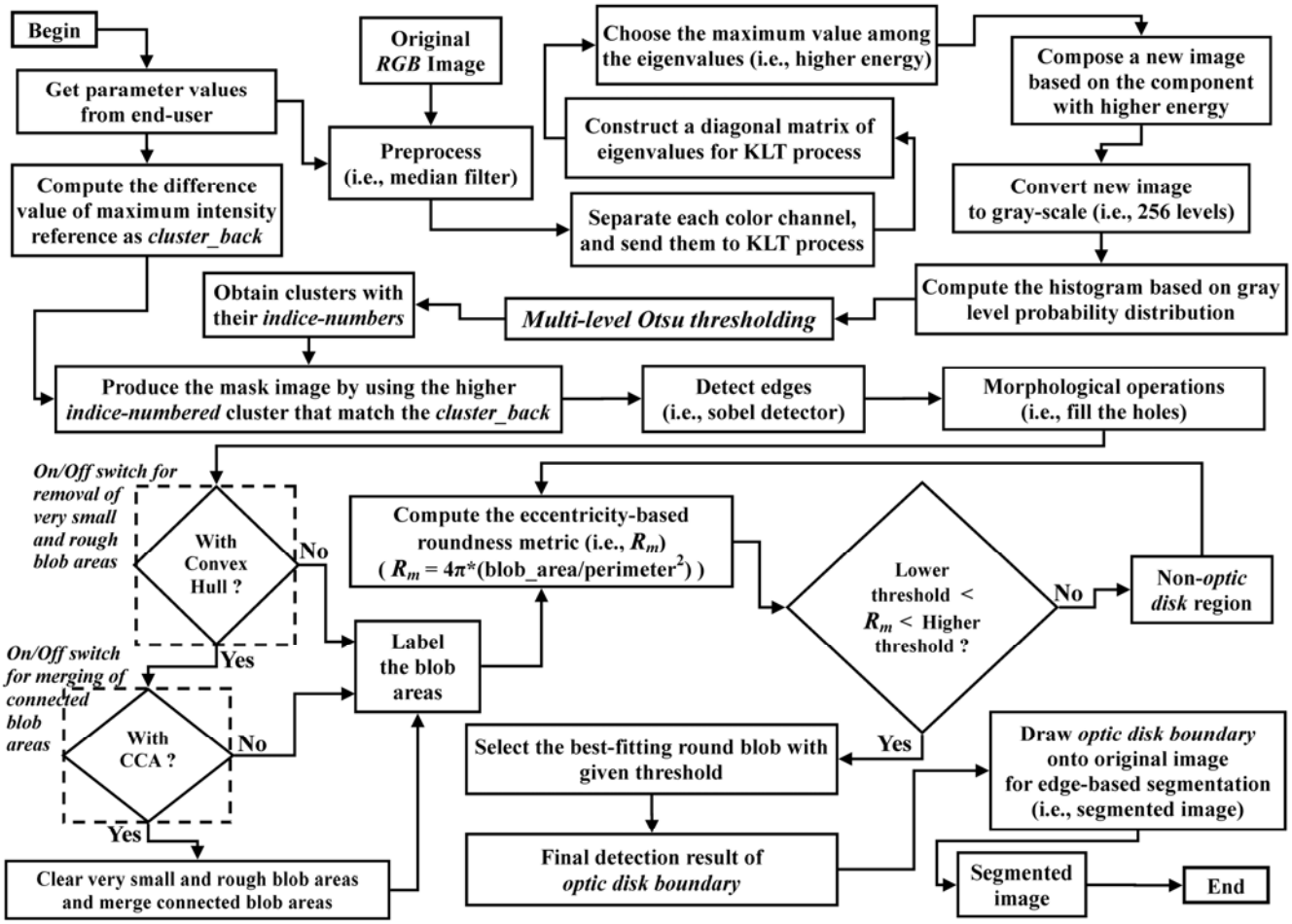

Figure 1. Flowchart of the proposed system for optic disk D&S

In our system, an original RGB retinal image is processed in pre-processing stage. A 9x9 median filter is applied to the image to remove some noises (noisy pixels as outliers) which came from digital fundus camera or some other sources. Then, the maximum intensity in given image is computed to serve as a maximum intensity reference. After this stage, each color channel of given image is separated, and also, they are sent to the KLT stage. Thence, the KLT process reduces the information of each image channels to a diagonal matrix of eigenvalues. Therefore, the maximum value among the eigenvalues (i.e., the component with the higher energy) is chosen to compose a new image. After this process, this new image is converted to gray-scale (i.e., 256 levels of intensity values).

In our study, we expect the OD to be one of the bright areas in a color retinal image, and thus, its boundaries are most significant proof of its location in that image. In this scope, we need to detect the brightest area in the image, and this is mostly done in the literature with the well-known gradient-based filter; namely the Sobel edge detector. Therefore, we also choose the Sobel edge detector for our study. For image segmentation, the result of a Sobel operator at each point in the image is either the corresponding gradient vector or the norm of the gradient vector. It is based on convolving the image with an integer-valued filter, which is small and separable. It performs a 2-dimensional spatial gradient quantity on a given image.

In OD D&S process, some detection difficulties occur due to high similarities to other large bright lesions in a given image. Besides, the multi-level Otsu thresholding segments the image into certain brightness regions. These regions correspond to one background and several objects. This process assumes that there are *N-1* thresholds, which divide the given original image into *N* classes. Therefore, it segments a gray level image into several separated regions. For Otsu's thresholding, the histogram based on the gray level probability distribution is computed by using this new image. The multi-level Otsu thresholding is applied on the gray scale image with its histogram by using proposed system, and thence, the clusters having different indices are obtained. The difference value between the maximum intensity reference and the intensity values of current clusters with their indice-numbers is computed, and also, it called as the *cluster_back* value. Consequently, a bi-level segmented (i.e., black-and-white) image is produced by using a cluster with a higher index that matches the *cluster_back* value. By using these values and Sobel edge detection, our proposed system determine the most luminous area with its boundaries defined as the chosen OD region.

In our study, we considered all pathological signs in any given image selected from three databases mentioned above. The *cluster_back* value is considered an indicator for OD region. The main reason for choosing a cluster with higher index based on its *cluster_back* value is the OD's brightness, because we expect the OD to be brighter than other regions (i.e., they contain the signs of pathology) in the color retinal image. This stands alone a figure of merit when dealing with those pathologies. Another proof is the eccentricity-based roundness of the OD region. Other regions, especially ones having pathological signs, have not a complete boundary or roundness value similar to the OD region identified in the GT data.

After the production of the mask image, our system obtains the edges in given mask image via Sobel edge detector. The edge map images are also produced by using the Sobel edge detector, thence, the holes in determined blob areas are filled with the help of the morphological operations, such as erosion and dilation with 3x3 rectangular structural element. Furthermore, from the programming point of view, the user is given only three options ("*remove very small areas from image*","*remove rough areas from image*" and "*merge connected areas in image*") in command window in MATLAB environment. These options/attributes take parameter values as user input (one or zero, indicating the current status of parameter (switch), i.e., on or off). In Fig. 1, a medical doctor or physician (the end-user) needs to know only about the status of abovementioned options, and then, the system works with pre-defined interval of *small_size* parameter values to clear small and rough areas with convex hull and to merge connected blob areas with CCA, respectively. In this step, a parameter (i.e., *small_size*) is checked by the system for the diameter of the blob areas in each given mask image that it is between 100 pixel and 950 pixel for DRIVE database, and between 100 pixel and 1500 pixel for STARE and DIARETDB1 databases.

The *small_size* parameter is identified to indicate the limit of coverage area of CCA for related regions. When the given blob area is smaller or larger than the *small_size* parameter value (i.e., diameter), then the system removes this blob area from the mask image. Consequently, the remaining blob areas (i.e., regions) in the mask image are labelled via region properties. These region properties are calculated by the use of the statistics based on the eccentricity, centroid, and bounding boxes of detected object(s). In a recursive computation, the eccentricity-based roundness metric is computed for each blob region in the mask image. In our system's infrastructure, the roundness metric R_m is identified as given below:

$$R_m = 4\pi\left(\frac{blob\_area}{perimeter^2}\right) \quad (1)$$

Then, our system tests the roundness metric value (R_m) that it is bigger than lower threshold value (i.e., 0.4) or lower than the higher threshold value (i.e., 0.95) in our study. In addition, the end-user may change the higher threshold value if necessary in a given test. If the test is failed, the given blob region is determined as *non-OD* region. When the test is successful, then our system selects the determined blob region as the best-fitting round blob (i.e., OD region) with given threshold. Thence, the final detection result of OD boundary is obtained. Consequently, for edge-based segmentation, the OD boundary is drawn onto original retinal image, thence, the OD region is segmented, and the segmented image (i.e., extracted OD region) is obtained by the system. In abovementioned process, *small_size* parameter value and roundness metric value (R_m) are significant values for the accuracy of D&S of OD region.

IV. Results and Discussion

In the present work, we used the images from the DRIVE [15, 25], STARE [16] and DIARETDB1 [17] retinal image databases to test the performance of our system. The subsets of these abovementioned databases are chosen usually by considering the signs of pathology, which has a direct effect on the overall performance of D&S algorithm. In addition, these subsets are frequently used in other studies in the literature for detection and segmentation of OD. For DIARET database, DIARETDB1 is especially encountered more frequently in the literature (as seen in the review part of this article).

The main reason of this choosing type is to compare our system's performance results with the ones from abovementioned studies' (i.e., ref. [18], [21], [23]). A total of 210 images was collected from three databases, where 141 of them had pathological signs or diseased areas.

Abovementioned three databases contain normal retinal images: namely, 33 images for DRIVE, 31 images for STARE and 5 images for DIARETDB1. They also contain retinal images with pathological signs: e.g. 7 images for DRIVE, 50 images for STARE and 84 images for DIARETDB1, as well.

In our study, the performance evaluation is made in two different way: qualitative and quantitative form. In the qualitative form, the final segmented image is evaluated by human expert. Also, this kind of evaluation is based on the human expert's previous experience. By the way, the final decision of human expert is almost relative due to the specific errors in the segmentation, and adhere to the human perception. In the quantitative form, there are some metrics to measure the system's performance, and they help to compute the total success rate of the system. In quantitative evaluation, the end-user has a chance in order to decide the accuracy of the segmentation as an overlap ratio between the final segmented object(s) in given image and a golden-standard (i.e., ground-truth, GT) data for given image. The GT data are usually defined by one or more human expert(s). Reference images are built up from GT data. In addition, the quantitative evaluation supports the detection or segmentation error rates that indicate the more realistic results of the segmentation obtained by the system.

In the study, we aim to show that a comparative analysis of the experimental results of our study via an objective evaluation. Our annotations of the images of the retina for GT data of OD is based on the hand-labeled marking. The performance of our system is evaluated by comparing a circular- or a patch-region limited by boundary of the OD with the same as marked independently by a human expert. This region limited by boundary of OD was drawn on each image of each given database, by magnifying the original image by 400% using the image manipulation software GIMP (The GNU Image Manipulation Program) [27]. The most attention on the drawing the region of the OD was paid so as to avoid the rim (i.e., boundary) of the sclera (i.e., scleral crescent or peripapillary atrophy [25]), which in some retinal images may be difficult to differentiate from the OD. In this way, we produced the GT data via labeling the pixels. As mentioned above, GT images in our study are treated as reference images which contains GT data, as well. In our GT images, there are two regions called as the OD region and the *non-OD* region. The pixels involved by the OD region are labeled as object, and the other pixels (i.e., the *non-OD* region) are labeled as background. Our GT images are given in the form in which they are *black-and-white*, and also, the pixels of foreground (i.e., object) are given as white, and the pixels of background are given as black in the image. In the following subsections, the details of the performance evaluation metrics, and the qualitative and quantitative results obtained in the experiments are given as well.

A. Performance evaluation

Some metrics used in the image segmentation literature are given as a similarity measure based on overlap ratio or equivalently as an error ratio. In our study, five selected metrics are applied to evaluate quantitatively the performance of proposed D&S system: Pixel-based Precision (P_P), Pixel-based Recall (P_R), Specificity ($Spec$), False Positive Rate (FPR), and Accuracy ($Accu$). In the scope of information retrieval, a contingency table involves the true positives (TP), true negatives (TN), false positives (FP) and false negatives (FN).

As a two-class classifier, this table aims to label pixels as *irrelevant* or *relevant* [28]. In the literature, P_P is a ratio as given below [29, 30]:

$$P_P = \frac{|TP|}{|TP| + |FP|} \tag{2}$$

where the $|\cdot|$ operator represents the number of pixels in the relevant area. In addition, the sensitivity (i.e., P_R) or the True Positive Rate (TPR) is given in a form similar to the one given as follows [29, 30]:

$$P_R = \frac{|TP|}{|TP| + |FN|} \tag{3}$$

The True Negative Rate (TNR) or $Spec$ is formulated as follows [29, 30]:

$$Spec = \frac{|TN|}{|TN| + |FP|} \tag{4}$$

The False Positive Rate (FPR) is defined by the formula given as below [29, 30]:

$$FPR = \frac{|FP|}{|FP| + |TN|} = (1 - Spec) \tag{5}$$

The $Accu$ is measured by the ratio of the total number of correctly classified pixels (sum of TP and TN) to the number of pixels in the camera's image FOV. $Accu$ is given as follows [10, 26]:

$$Accu = \frac{|TP| + |TN|}{|TP| + |FP| + |TN| + |FN|} \tag{6}$$

Abovementioned metrics are in range $[0,1]$. For four metrics, i.e. P_P, P_R, $Spec$, and $Accu$, the *zero* value and the *one* value indicate the *worst* result and the *best* result for performance measurement, respectively. On the contrary, for the pixel error-based metric, i.e. FPR, the *zero* value and the *one* value indicate the *best* result and the *worst* result for performance measurement, respectively. According to Fraz et al. [26], one can decide to use a receiver operating characteristic (ROC) curve for performance evaluation that it plots the fraction of OD pixels correctly classified as OD region, (i.e., TPR), versus the fraction of *non-OD* pixels wrongly classified as OD, (i.e., FPR). The closer the curve approaches the top left corner in the plot, the better is the performance of the system. For retinal images, the TPR and FPR are computed considering only pixels inside the camera's image FOV.

The FPR calculation involves also false positive values (i.e., FPs), but the FP values indicate only the number of *non-OD* region pixels that are incorrectly identified as OD region pixels. As in any image from three abovementioned retinal image databases, there are much more *non-OD* region's pixels than OD region's pixels. The main reason for the latter is the existing large pathological signs and non-removable noises in these images. Hence, FPR is the

number of negative instances (i.e., *non-OD* pixels) that were erroneously reported as being positive (i.e., OD pixels).

B. Performance results

In our study, the OD region was manually delineated in each retinal image by human expert. Furthermore, these hand-marked images were used as reference that the GT used to evaluate the performance of our D&S system. In our experiments, the retinal images of each database are used to detect and segment the OD region in a fully-automatic manner. Our tests are executed over 10 trials with given test parameters for each one of the retinal images of abovementioned three databases. In a given test run with an original image, the end-user may select some different parameter values to test the system or to improve the performance obtained by the system, at the end of the test run, the system produces the segmented mask image and the resultant image of final segmentation. The resultant (i.e., edge-based segmented) image is evaluated both in qualitative and quantitative way.

In quantitative way, it is evaluated by using related GT image file. In this way, the evaluation is based on the pixel-by-pixel comparison between the regions of both segmented mask and GT images. The overlap ratio of the regions are treated as the similarity or error ratios (i.e., performance measurement) of OD segmentation of the system. In addition, the metrics and the obtained measurements are given as simple statistics based on the information retrieval. According to the study of Zhu et al. [25], abovementioned overlap ratio is computed as follows:

$$Overlap = \frac{S_1 \bigcap S_2}{S_1 \bigcup S_2} \tag{7}$$

where S_1 is the region marked by human expert and S_2 is the region detected by the proposed system. In addition, the value of overlap is limited to the range $[0,1]$. The overlap ratio is defined to measure the common area between the OD region in the GT image and the OD region in the segmented mask image. This segmented mask image is produced by our system. Therefore, overlap ratio is used to detect OD localization. The *small_size* values are given in the pixel area range $[100, 950]$ for DRIVE database, and in the pixel area range $[100, 1500]$ for STARE and DIARETDB1 databases. In our experiments, there are optimally 24 indexed clusters (i.e., cluster with its indice number). The difference value between the maximum intensity reference and the intensity values of current clusters with their indice-numbers is presented by the *cluster_back* value. For example, if *cluster_back* is given as 5, then the maximum intensity reference is detected by the system in the cluster with 19^{th} indice number. The parameter sets used in our experiments on the DRIVE, STARE and DIARETDB1 databases are given in the supplementary materials of this paper. For details of related parameters of the system, the reader may refer to the supplementary materials given at related website [31].

Our system's OD localization (i.e., OD-center detection) is tested in our experiments that OD is successfully detected by the system in all 40 images from DRIVE database (i.e., with success rate of 100%), in all 89 images from DIARETDB1 database (i.e., with success rate of 100%), and in 76 out of 81 images from STARE database (i.e., with success rate of 93.82%). The system's overall success rate for OD localization is 97.94%, which is an averaged value over abovementioned three retinal image databases. It should be noted that we considered as correct all automatically detected OD localization that are within the borders of the OD marked manually by human expert.

In Fig. 2, Fig. 3, and Fig. 4, the original, GT, and segmented mask images are shown in relevant columns, where the qualitative results are shown as segmented mask images. In these figures, the GT images are given as a reference of performance evaluation. The selected images used in these figures are randomly chosen to show the experimental results. In the final segmented images from abovementioned three databases images, the boundary of OD region detected by our system is indicated with a white boundary line.

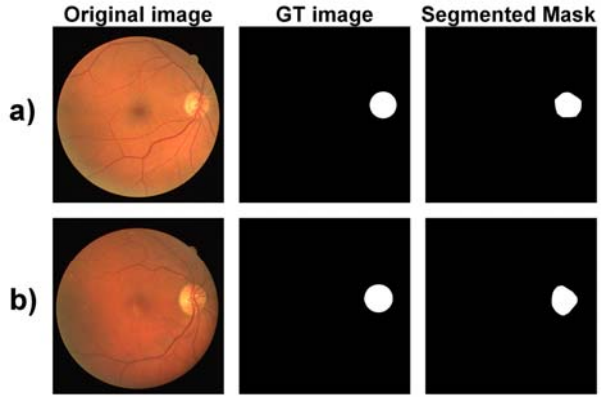

Figure 2. Qualitative results for DRIVE database, a)"16_test", and b)"25_training" images

In Fig. 2, a)"16_test" and b)"25_training" images are shown. In the figure, the segmented masks are very similar to the GT images (i.e., according to the human expert, it is a *good* result for qualitative performance evaluation), but the segmented OD region in segmented mask image of "25_training" is smaller than the expected OD region's circle in GT image due to the under-segmentation problem (i.e., a *bad* segmentation result for qualitative performance evaluation).

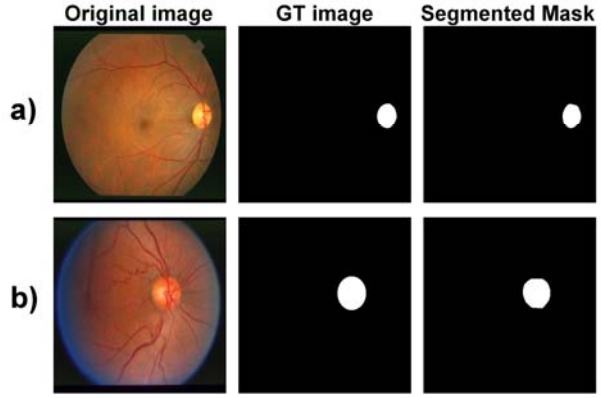

Figure 3. Qualitative results for STARE database, a)"im0076", and b)"im0241" images

In Fig. 3, a)"im0076" and b)"im0241" images are shown. In the figure, the segmented masks are very similar to the

GT images. It indicates a *good* result for qualitative performance evaluation. In Fig. 4, a)"image005" and b)"image016" images are shown. In the figure, the segmented masks are very similar to the GT images. It indicates a *good* result for qualitative performance evaluation. In our experiments, overall quantitative performance results are calculated over 40 images of DRIVE database, over 81 images of STARE database, and over 89 images of DIARETDB1 database. These results are treated as the mean values of total measurements in related experiments, and also, they are given as performance percentage ratio.

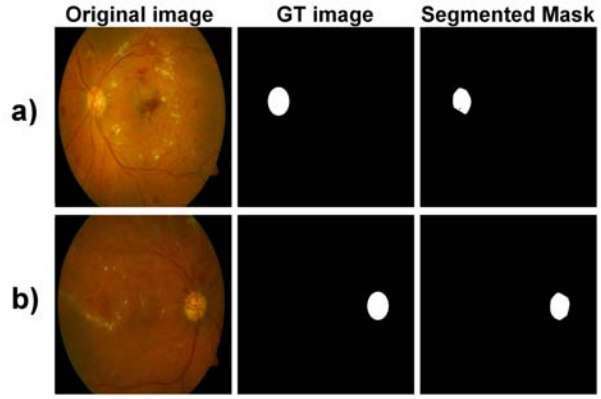

Figure 4. Qualitative results for DIARETDB1 database, a)"image005", and b)"image016" images

In this way, for abovementioned three retinal image databases, the average values for overall quantitative performance results of OD segmentation over three databases are given in Table I. Some methods or systems in the literature are affected generally by poor contrast in images, complicating the OD detection due to the presence of large bright lesions. The large bright artifacts, resulting from a bad retinal image acquisition, further affect the OD detection. Nevertheless, our system produces quite good qualitative results for D&S of OD. It can be seen in Fig. 2 to Fig. 4 that our system overcomes these characteristic problems of the retinal images stemming from the screening or acquisition programs.

TABLE I. OVERALL QUANTITATIVE SEGMENTATION PERFORMANCE RESULTS FOR THREE RETINAL IMAGE DATABASES USED IN THE EXPERIMENTS

Database name	P_P	P_R	*Spec*	*FPR*	*Accu*
DRIVE	98.88%	99.91%	56.74%	43.25%	98.83%
STARE	98.62%	97.38%	49.69%	50.30%	96.11%
DIARETDB1	99.29%	99.90%	56.88%	43.11%	99.20%
Average performance results	98.93%	99.06%	54.43%	45.55%	98.04%

In Table II, a comparison of OD detection performance results in our experiments with other works in the literature related to three retinal image databases is shown. As it can be seen from Table II, our system in general outperforms the works developed by Qureshi et al. [21] and Welfer et al. [23] in detecting the OD in images of DIARETDB1 database. In addition, the OD detection results achieved with the DRIVE database are the same as the results obtained with other works as given in Table II.

TABLE II. COMPARISON OF OD DETECTION PERFORMANCE RESULTS IN THE EXPERIMENTS WITH OTHER WORKS IN THE LITERATURE

Study	Success rate of OD localization	Database name
Youssif et al. [18]	98.77%, 100%	STARE, DRIVE.
Qureshi et al. [21]	96.79%, 94.02%, 100%	DIARETDB0, DIARETDB1, DRIVE.
Welfer et al. [23]	97.75%, 100%	DIARETDB1, DRIVE.
Our study	100%, 93.82%, 100%	DRIVE, STARE, DIARETDB1.

In terms of OD D&S, the proposed system is robust in the presence of uneven illumination and clusters of exudates which may have the same characteristics of the OD region, and other artifacts.

As mentioned before, the combined system of Qureshi et al. [21] achieved an overall performance result for OD detection over DRIVE and DIARETDB1 databases that is given as the total average performance is 97.01% (i.e., with success rate of 100% on the DRIVE database and of 94.02% on the DIARETDB1 database).

In addition, the proposed method of Welfer et al. [23] achieved an overall performance result for OD detection over DRIVE and DIARETDB1 databases that is given as the total average performance is 98.87% (i.e., with success rate of 100% on the DRIVE database and of 97.75% on the DIARETDB1 database). However, our system's overall performance result for OD detection over abovementioned two databases is 100% (i.e., both with success rate of 100% on the DRIVE and DIARETDB1 databases). In this frame, the aim of our study was to give a better understanding of our system in term of improving the D&S performance as compared to individual methods.

The proposed algorithm of Morales et al. [22] has a specific OD segmentation stage. In this stage, the centroid calculation, the stochastic watershed transformation and the region discrimination are given as sub-stages of the segmentation stage. In addition, the region of interest (ROI) for segmentation process has been obtained in this segmentation stage. In the post-processing stage, they determined the OD contour via a circular approximation. In their study, they also discussed about the reason for which a circular approximation is applied on the segmented disc that is due to the complexity of the fundus images. Thence, the high number of elements of fundus images makes a perfect segmentation difficult.

On the contrary, our system does not require a specific ROI, and an extra circular approximation (or any post-processing stage) during the D&S process. Furthermore, a post-processing stage can potentially increase the computational time cost for large image databases. In our system, the CCA and convex hull encapsulation are given as the OD segmentation's in-build parts (as seen in the related parts of the Fig. 1) that are chosen selectively by end-user. Moreover, our system is not influenced by the outgoing blood vessels crossing the OD, and also, it tries to detect and segment the OD, without assuming any pre-defined shape or region. Our system only checks the roundness metric (i.e., R_m) as a threshold value for eccentricity.

In Fig. 5, Fig. 7, and Fig. 9, the P_P vs. P_R curve plot for abovementioned three databases are shown, respectively. The closer the curve approaches the top right corner in the plot, the better is the performance of the system. It is clearly seen from the plot, our system has a good performance result for OD D&S of given datasets of retinal images.

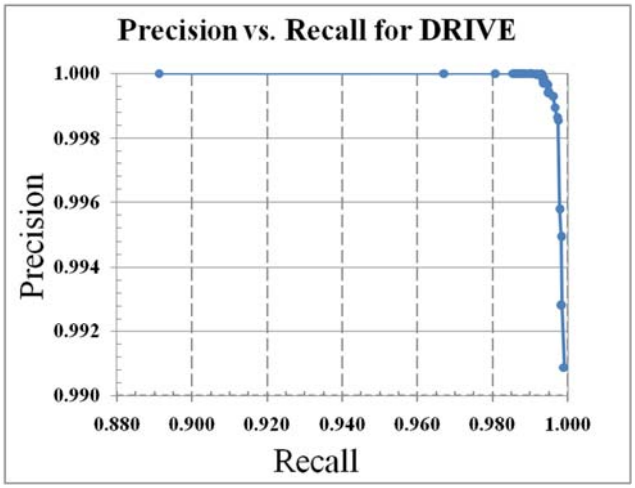

Figure 5. Precision (P_P) vs. Recall (P_R) curve for our experiments on DRIVE database

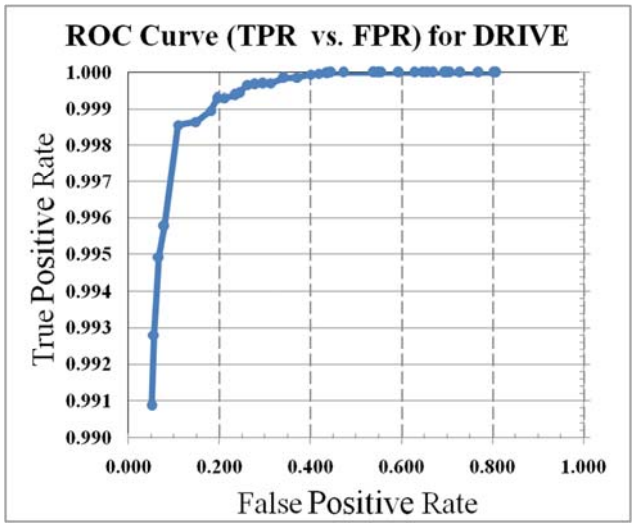

Figure 6. ROC curve for our experiments on DRIVE database

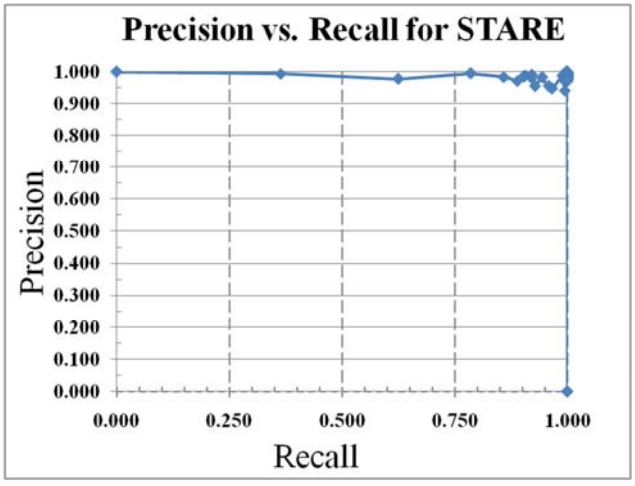

Figure 7. Precision (P_P) vs. Recall (P_R) curve for our experiments on STARE database

In Fig. 6, Fig. 8, and Fig. 10, the *TPR* vs. *FPR* curve (i.e., ROC curve) plot for abovementioned three databases are shown, respectively. As mentioned before, the closer the curve approaches the top left corner in the plot, the better is the performance of the system. Similarly, our system has a good performance result for OD D&S as well.

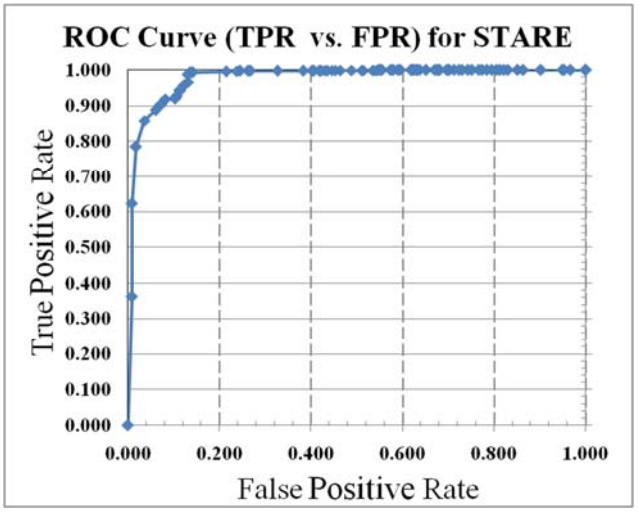

Figure 8. ROC curve for our experiments on STARE database

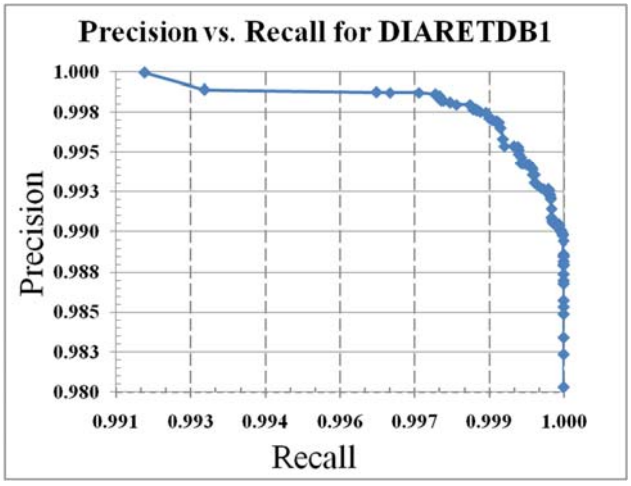

Figure 9. Precision (P_P) vs. Recall (P_R) curve for our experiments on DIARETDB1 database

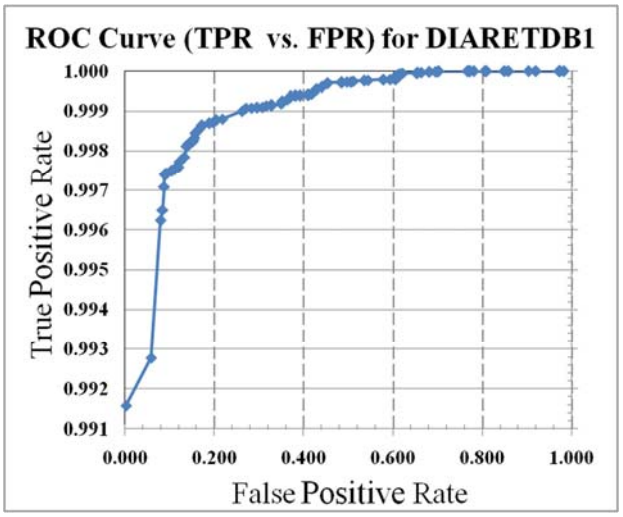

Figure 10. ROC curve for our experiments on DIARETDB1 database

Our system is implemented on the MATLAB numerical computing environment, and the experimental tests are runned on a Microsoft Windows 7 (64-bit) OS machine equipped with Intel(R) Core(TM) i7 CPU (i.e., Quad-core) at 3.20 GHz and 12.0 Gbytes of RAM.

At the processing of each image from abovementioned three retinal image databases, the computational time of our system is approximately between 40 and 170 seconds, which is measured by the MATLAB environment, as well.

In their study, Youssif et al. [18] implemented a MATLAB prototype for the procedure applying the matched filters, where runs needed on average 3.5 min for each image. Utilization of two-dimensional matched filters leads to a higher number of computations as compared to the other methods reviewed in the literature [18].

According to the study of Welfer et al. [23], the required average processing time per image is between 22.86 and 528.16 seconds, which were performed by using retinal images from DRIVE and DIARETDB1 databases, respectively. These values are computed by using the computational times in [23] that are given in a comparison table. It represents the computational costs for DRIVE and DIARETDB1 databases that are obtained by seven studies in the literature. In this scope of complexity, our system can be seen as an alternative way to process retinal image datasets in the literature.

In Fig. 11, the final edge-based segmented images from DRIVE database, a)"01_test", b)"04_test", c)"07_test", d)"09_test", e)"16_test", f)"25_training", g)"27_training", h)"33_training", i)"36_training", j)"38_training" images are shown. Other than the (edge-based) segmented "07_test" image (i.e., *bad* segmentation result), all images have very similar boundary to related GT image's OD region's boundary (i.e., *good* segmentation result).

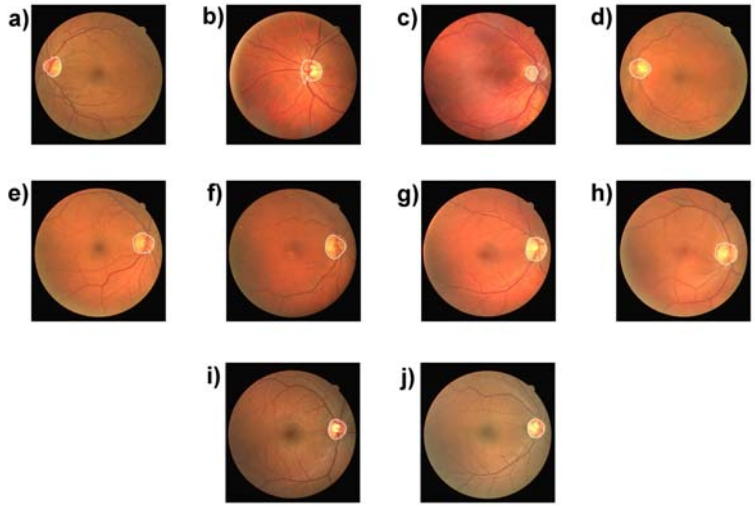

Figure 11. Final segmented images for DRIVE database, a)"01_test", b)"04_test", c)"07_test", d)"09_test", e)"16_test", f)"25_training", g)"27_training", h)"33_training", i)"36_training", j)"38_training" images

In Fig. 12, the final edge-based segmented images from STARE database, a)"im0002", b)"im0037", c)"im0042", d)"im0049", e)"im0076", f)"im0139", g)"im0170", h)"im0241", i)"im0245", j)"im0319" images are shown. In the figure, the "im0002", "im0037", "im0042" and "im0049" images have *bad* segmentation results due to the under-segmentation problem, but other images have very similar boundary to related GT image's OD region's boundary, and also, the others have a *good* segmentation result for qualitative performance evaluation.

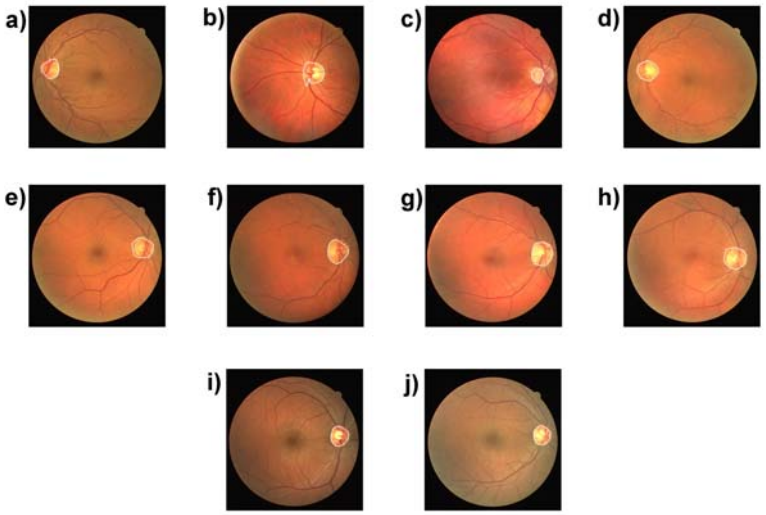

Figure 12. Final segmented images for STARE database, a)"im0002", b)"im0037", c)"im0042", d)"im0049", e)"im0076", f)"im0139", g)"im0170", h)"im0241", i)"im0245", j)"im0319" images

In Fig. 13, the final edge-based segmented images from DIARETDB1 database, a)"image005", b)"image016", c)"image017", d)"image024", e)"image031", f)"image039", g)"image049", h)"image063", i)"image070", j)"image081" images are shown. In the figure, the "image005", "image031", "image049", "image063" and "image081" images have *bad* segmentation results due to the under-segmentation or over-segmentation problem, but other images have very similar boundary to related GT image's OD region's boundary, and also, the others have a *good* segmentation result for qualitative performance evaluation.

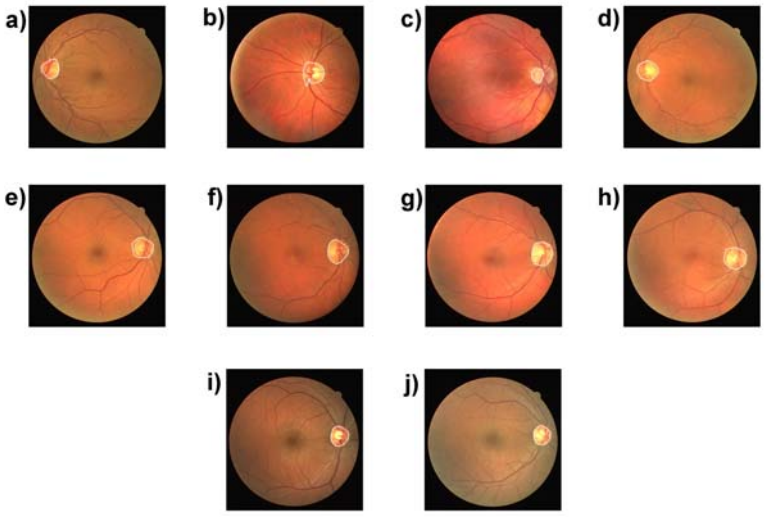

Figure 13. Final segmented images for DIARETDB1 database, a)"image005", b)"image016", c)"image017", d)"image024", e)"image031", f)"image039", g)"image049", h)"image063", i)"image070", j)"image081" images

V. Conclusion

The proposed system consists of well-known methods as KLT, multi-level Otsu's thresholding and Sobel edge detection. Moreover, these methods in this order have never been used for OD D&S in the literature. The main contribution of our study is to develop an automatic (i.e., unsupervised) and accurate OD D&S system with lower computational complexity. This system can be seen as an interesting option to handle retinal image datasets. In terms of the OD localization and segmentation accuracy, this system is more preferable than extending the semi-automatic or manual D&S systems.

In this frame, its first application to color retinal images is introduced and systemically tested. In addition, our system does not require a vessels elimination sub-stage in D&S process in order to reduce the vessels influence in the OD location or in the determination of its boundary (i.e., OD contour).

With the aim of improved diagnosis of retiono-pathologies, the extraction of prominent features is important for the accurate D&S in retinal fundus images, such as the optic nerve head (i.e., OD), fovea, and blood vessels. In our study, the system's overall OD segmentation accuracy was computed for all three abovementioned databases with an average of about 98.04%, which was already given in Table I. Furthermore, the system's overall detection rate of OD (i.e., OD localization) was computed for all three databases with an average of about 97.94%, which was based on the values taken from Table II. In this way, the performance of system based on accuracies and detections were calculated over all 210 images. Therefore, these results suggest that our system is able to detect and segment the OD more accurately than most of the other methods/systems presented in the literature.

In consequence, these results indicate that our system appears to be robust to the different imaging conditions and situations existing in abovementioned retinal image databases, such as varying image quality, illumination, and other artifacts. The quantitative evaluation of D&S results for our proposed system show that our system should also be useful to researchers in various areas of retinal image modeling and analysis. Our system performed well with images of the DRIVE, STARE and DIARETDB1 databases. These three databases are compounded of more diverse and realistic set of images, regarding intra- and inter-variations and the existence of lesions.

In further study, we plan to add new segmentation methods and other edge detection techniques into our system, and also, we plan to try other retinal image databases for performance tests.

References

[1] S. Sekhar, W. Al-Nuaimy and A. K. Nandi, "Automated localisation of retinal optic disk using Hough transform", In Proc. 5th IEEE International Symposium on Biomedical Imaging: From Nano to Macro (ISBI 2008), Paris, France, 2008. pp. 1577-80. [Online]. Available: http://dx.doi.org/10.1109/ISBI.2008.4541312

[2] D. Welfer and J. Scharcanski, C. M. Kitamura, M. M. Dal Pizzol, L. W. B. Ludwig, D. R. Marinho, "Segmentation of the optic disk in color eye fundus images using an adaptive morphological approach", Comput Biol Med, vol. 40, no. 2, pp. 124-137, 2010. [Online]. Available: http://dx.doi.org/10.1016/j.compbiomed.2009.11.009

[3] M. Niemeijer, M. D. Abràmoff and B. V. Ginneken, "Fast detection of the optic disc and fovea in color fundus photographs", Medical Image Analysis, vol. 13, no. 6, pp. 859-870, 2009. [Online]. Available: http://dx.doi.org/10.1016/j.media.2009.08.003

[4] C. Duanggate, B. Uyyanonvara, S. S. Makhanov, S. Barman and T. Williamson, "Parameter-free optic disc detection", Comput Med Imaging Graph, vol. 35, no. 1, pp. 51-63, 2011. [Online]. Available: http://dx.doi.org/10.1016/j.compmedimag.2010.09.004

[5] H. F. Jelinek, C. Depardieu, C. Lucas, D. Cornforth, W. Huang and M. J. Cree, "Towards vessel characterisation in the vicinity of the optic disc in digital retinal images", in Proc. the image and vision computing conference, Otago, New Zealand, 2005.

[6] A. Osareh, M. Mirmehdi, B. Thomas and R. Markham, "Colour morphology and snakes for optic disc localisation", in Proc. the 6th medical image understanding and analysis conference, A. Houston and R. Zwiggelaar (editors), BMVA Press, pp. 21-24, 2002.

[7] D. Kavitha and D. S. Shenbaga, "Automatic detection of optic disc and exudates in retinal images", in Proc. IEEE Int. conf. on intelligent sensing and information processing (ICISIP 2005), pp. 501-506, 2005.

[8] K. W. Tobin, E. Chaum, V. P. Govindasamy, T. P. Karnowski and O. Sezer, "Characterization of the optic disc in retinal imagery using a probabilistic approach", in Proc. SPIE International Symposium on Medical Imaging, San Diego, California, USA, vol. 6144:61443F, 2006.

[9] P. C. Siddalingaswamy and P. K. Gopalakrishna, "Automatic Localization and Boundary Detection of Optic Disc Using Implicit Active Contours", International Journal of Computer Applications, vol. 1, no. 6, pp. 1-5, 2010.

[10] C. Köse, U. Şevik, C. İkibaş and H. Erdöl, "Simple methods for segmentation and measurement of diabetic retinopathy lesions in retinal fundus images", Comput Methods Programs Biomed, vol. 107, no. 2, pp. 274-293, 2012. [Online]. Available: http://dx.doi.org/ 10.1016j.cmpb.2011.06.007

[11] C. Muramatsu, T. Nakagawa, A. Sawada, Y. Hatanaka, T. Hara, T. Yamamoto and H. Fujita, "Automated segmentation of optic disc region on retinal fundus photographs: Comparison of contour modeling and pixel classification methods", Comput Methods Programs Biomed, vol. 101, no. 1, pp. 23-32, 2011. [Online]. Available: http://dx.doi.org/10.1016/j.cmpb.2010.04.006

[12] H.-F. Ng, "Automatic thresholding for defect detection", Pattern Recogn Letters, vol. 27, no. 14, pp. 1644-1649, 2006. [Online]. Available: http://dx.doi.org/10.1016/j.patrec.2006.03.009

[13] D.-Y. Huang, T.-W. Lin and W.-C. Hu, "Automatic Multilevel Thresholding Based On Two-Stage Otsu's Method With Cluster Determination By Valley Estimation", International Journal of Innovative Computing, Information and Control, vol. 7, no. 10, pp. 5631-5644, 2011.

[14] N. Otsu, "A Threshold Selection Method from Gray-level Histograms", IEEE Trans. on Syst. Man Cybern, vol. 9, pp. 62-66 , 1979.

[15] M. Niemeijer and B. V. Ginneken, "Digital Retinal Images for Vessel Extraction image (DRIVE) database", 2002, [Online]. Available: http:// www.isi.uu.nl/Research/Databases/DRIVE

[16] A. Hoover, "STructured Analysis of the Retina (STARE) database", 2000, [Online]. Available: http://www.parl.clemson.edu/~ahoover/stare

[17] T. Kauppi, V. Kalesnykiene, J. K. Kamarainen, L. Lenu, I. Sorri, A. Raninen, R. Voutilainen, J. Pietilä, H. Käluiäinen and H. Uusitalo, "Diaretdb1 Diabetic Retinopathy Database and Evaluation Protocol", in Proc. the Medical Image Understanding and Analysis, Aberystwyth, UK, pp. 61-65, 2007.

[18] A. A. A. Youssif, A. Z. Ghalwash and A. A. S. A. Ghoneim, "Optic Disc Detection From Normalized Digital Fundus Images by Means of a Vessels' Direction Matched Filter", IEEE Trans Med Imaging, vol. 27, no. 1, pp. 11-18 , 2008.

[19] M. Niemeijer, B. V. Ginneken, F. B. terHaar and M. D. Abràmoff, "Automatic detection of the optic disc, fovea and vascular arch in digital color photographs of the retina", in Proc. the British Machine Vision Conference, pp. 17.1-17.10, 2005. [Online]. Available: http://dx.doi.org/10.5244/C.19.17

[20] T. Walter and J. C. Klein, "Segmentation of color fundus images of the human retina: Detection of the optic disc and the vascular tree using morphological techniques". in Proc. Second International Symposium of Medical Data Anlaysis (ISMDA), pp. 282-287, 2001.

[21] R. J. Qureshi, L. Kovacs, B. Harangi, B. Nagy, T. Peto and H. Hajdu, "Combining algorithms for automatic detection of optic disc and macula in fundus images", Computer Vision and Image Understanding, vol. 116, no. 1, pp. 138-145, 2012. [Online]. Available: http://dx.doi.org/10.1016/j.cviu.2011.09.001

[22] S. Morales, V. Naranjo, J. Angulo and M. Alcañiz, "Automatic Detection of Optic Disc Based on PCA and Mathematical Morphology", IEEE Trans Med Imaging, vol. 32, no. 4, pp. 786-796, 2013.

[23] D. Welfer, J. Scharcanski and D. R. Marinho, "A Morphologic two-stage approach for automated optic disk detection in color eye fundus images". Pattern Recogn Letters, vol. 34, no. 5, pp. 476-485, 2013. [Online]. Available: http://dx.doi.org/10.1016/j.patrec.2012.12.011

[24] P.-S. Liao, T.-S. Chen and P.-C. Chung, "A fast algorithm for multilevel thresholding", Journal of Information Science and Engineering, vol. 17, no. 5, pp. 713-727, 2001.

[25] X. Zhu, R. M. Rangayyan and A. L. Ells, "Digital Image Processing for Ophthalmology: Detection of the Optic Nerve Head", Synthesis Lectures on Biomedical Engineering, Morgan & Claypool Publishers, vol. 6, no. 1, pp. 1-106, 2011.

[26] M. M. Fraz, P. Remagnino, A. Hoppe, B. Uyyanonvara, A. R. Rudnicka, C. G. Owen and S. A. Barman, "Blood vessel segmentation methodologies in retinal images – A survey", Comput Methods Programs Biomed, vol. 108, no. 1, pp. 407-433, 2012. [Online]. Available: http://dx.doi.org/10.1016/j.cmpb.2012.03.009

[27] The GNU Image Manipulation Program website, 2014, [Online]. Available: http://www.gimp.org

[28] C. D. Manning, P. Raghavan and H. Schütze, "Introduction to Information Retrieval", Draft Online Copy (2009.04.01), Cambridge University Press, New York, NY, USA, 2009. [Online]. Available: http://nlp.stanford.edu/IR-book/pdf/irbookprint.pdf

[29] A. Baumann, M. Boltz, J. Ebling, M. Koenig, H. S. Loos, M. Merkel, W. Niem, J. K. Warzelhan and J. Yu, "A review and comparison of measures for automatic video surveillance systems", EURASIP Journal on Image and Video Processing, Article ID: 824726, pp. 1–30, 2008. [Online]. Available: http://dx.doi.org/10.1155/2008/824726

[30] B. Karasulu, "An Approach Based on Simulated Annealing to Optimize the Performance of Extraction of the Flower Region using Mean-Shift Segmentation", Applied Soft Computing, vol. 13, no. 12, pp. 4763-4785, 2013. [Online]. Available: http://dx.doi.org/10.1016/j.asoc.2013.07.019

[31] The OD D&S Program website, 2014, [Online]. Available: http://members.comu.edu.tr/bkarasulu/ODDS